Lithos 388–389 (2021) 106021

Contents lists available at ScienceDirect

Lithos

journal homepage: www.elsevier.com/locate/lithos

Research Article

Simultaneous development of arc-like and OIB-like mafic dikes in eastern Guangdong, SE China: Implications for late Jurassic – early Cretaceous tectonic setting and deep geodynamic processes of South China

Qing-He Yan [a,b,c,d], He Wang [a,b,*], Yangming Wu [e,f,**], Guoxiang Chi [c]

[a] CAS Key Laboratory of Mineralogy and Metallogeny, Guangzhou Institute of Geochemistry, Chinese Academy of Sciences, Guangzhou 510640, China
[b] CAS Center for Excellence in Deep Earth Science, Guangzhou, 510640, China
[c] Department of Geology, University of Regina, Regina, Saskatchewan S4S 0A2, Canada
[d] State Key Laboratory of Isotope Geochemistry, Guangzhou Institute of Geochemistry, Chinese Academy of Sciences, Guangzhou 510640, China
[e] School of Earth Sciences and Engineering, Sun Yat-Sen University, Guangzhou, China
[f] Southern Marine Science and Engineering Guangdong Laboratory (Zhuhai), Zhuhai, China

ARTICLE INFO

Article history:
Received 19 October 2020
Received in revised form 10 January 2021
Accepted 26 January 2021
Available online 31 January 2021

Keywords:
Jurassic Arc-like lamprophyre
Simultaneous Arc- and OIB-like Cretaceous mafic dikes
Initial roll-back
Paleo-Pacific plate subduction
Tectonic setting, South China

ABSTRACT

The Mesozoic South China is characterized by extensive magmatism, transition from Jurassic intraplate magmatism to Cretaceous active continental margin magmatism. However, the time and deep geodynamic processes accounting for the Mesozoic magmatism remains controversial. In this study, we presented new SIMS zircon U—Pb ages, in-situ Sr isotope of plagioclase, whole-rock geochemical and Sr–Nd–Pb isotopic data on three suites of mafic dikes in eastern Guangdong, namely Anliu (AL) and Sanjiaowo (SJW) and Jishuimen (JSM) mafic dikes. The AL (154.3 ± 3.4 Ma) and SJW (141.3 ± 4.0 Ma and 143.2 ± 2.3 Ma) dikes show arc-like geochemistry and "crust-like" isotopic signatures, likely derived from partial melting of a subduction metasomatized lithospheric mantle. Meanwhile, the JSM dikes (141.7 ± 3.2 Ma) exhibit OIB-type geochemical and isotopic features, and were likely derived from partial melting of an enriched asthenospheric mantle. The development of late Jurassic AL lamprophyre may represent the oldest Paleo-Pacific subduction-related arc-type mafic rocks so far recorded in South China. Development of dikes (SJW vs JSM) with different geochemical signatures (Arc vs OIB) at the same time within a limited space indicates that asthenosphere-related process overprint and co-operate with subduction-related magmatism and imply the initiation of Paleo-Pacific subduction roll-back was potentially at least ca.141 Ma.

1. Introduction

The Mesozoic South China geology is characterized by extensive magmatism and Sn—W mineralization, forming a ca. 600 km wide magmatic belt (Fig. 1). Previous studies show that Jurassic (early Yanshanian) magmatism is mainly located in the interior South China (e.g., Nanling Range) and Cretaceous (late Yanshanian) magmatism is mainly distributed along the South China coastal region (Guo et al., 2012; Li and Li, 2007). Although it has long been suggested that South China was influenced by the Paleo-Pacific subduction tectonics in various ways e.g., a normal subduction (e.g., Jahn et al., 1990); subduction with gradually dipping angles (Zhou and Li, 2000); foundering of a flat-slab subduction (Li and Li, 2007); and slab tearing or window opening within the subducting Plate (Mao et al., 2013), at least since the Middle Jurassic (e.g., Zhou et al., 2006; Liu et al., 2012), actually no typical subduction-related mafic rocks older than ~128 Ma (Li et al., 2018) and the absence of coeval arc-type andesitic magmatism in South China make some other workers argue that the Paleo-Pacific subduction did not commence before the Cretaceous (e.g., Veevers, 2004; Chen et al., 2008). And they attributed the Early Yanshanian (Jurassic) magmatism in South China to (i) post-collisional extension of the Triassic Indosinian orogeny (e.g., Chen et al., 2008), or (ii) intra-continental extension (in response to asthenospheric upwelling) (e.g., Gan et al., 2018).

Meanwhile, it is well known that there is a general change of tectonic regime from compressional to extensional in late Jurassic to early Cretaceous (Wong et al., 2009; Liu et al., 2015a; Zhou et al., 2016), and the Cretaceous voluminous felsic volcanism is generally interpreted to be related to Paleo-Pacific subduction, yet the starting time and nature of this transition and the deep processes associated with it are still debatable and not well understood (e.g., Wong et al., 2009; Liu et al., 2015a; Zhou et al., 2016). A subsequently slab roll-back in the Late Jurassic–Cretaceous after

* Correspondence to: He Wang, CAS Key Laboratory of Mineralogy and Metallogeny, Guangzhou Institute of Geochemistry, Chinese Academy of Sciences, Guangzhou 510640, China.
** Corresponding author at: School of Earth Sciences and Engineering, Sun Yat-Sen University, Guangzhou, China;
E-mail address: wanghe@gig.ac.cn (H. Wang).

https://doi.org/10.1016/j.lithos.2021.106021
0024-4937/

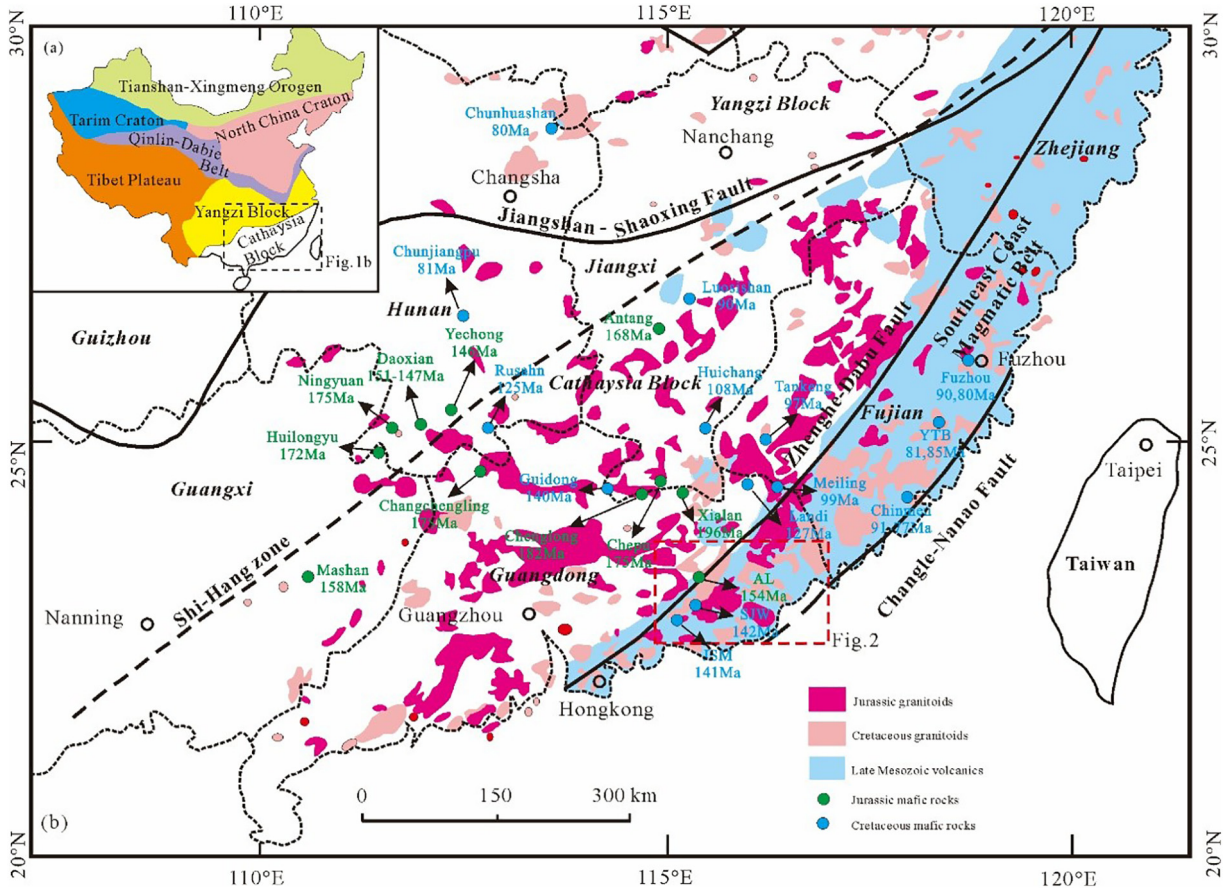

Fig. 1. (a) Tectonic map of China; (b) Simplified geologic map of South China, showing the distributions of Mesozoic granitoids, mafic rocks and volcanics (modified after Zhou et al., 2006; Liu et al., 2012; Meng et al., 2012).

slab foundering" of the retreating flat subduction in South China was proposed by Li and Li (2007). Wong et al. (2009) proposed the Baijuhuajian A-type granite (125 Ma) was generated due to the roll-back of the subducted paleo-Pacific Plate and may define the initial time of the extension. Yang et al. (2012) reported that the A-type granites (137 to 122 Ma) in the Gan–Hang belt formed in back-arc extension or intra-arc rift settings, and proposed that the initial extension may start at ca. 137 Ma. Liu et al. (2014) examined the extensive Cretaceous volcanic rocks in the coastal area of South China, and speculate the initial roll-back occurred at ca. 130 Ma. Whereas, detail petrology, geochronology, and geochemistry study suggest that the Late Yanshanian magmatism in the coastal area was caused by slab break-off of the Paleo-Pacific Plate during the Cretaceous and the starting time of extension is at ca. 125 Ma (Li et al., 2014). The lack of constraints in the Mesozoic regional tectonics is partly led by the inadequate knowledge on the Mesozoic lithospheric mantle in South China, because previous studies mostly focused on the granites and their volcanic counterparts in South China, which could not provide good constrains on the nature and evolution of the deep-sated processes.

Mafic dike swarms are commonly formed by mafic magma injection under local or regional extension (e.g., Eby, 1992; Mathieu et al., 2008). They contain more useful information about the nature of the magma source and tectonic setting than granitoids. Mesozoic mafic dikes are widespread and studied for decades in South China, with a variety of geochemical signatures indicating different sources and deep-seated processes (e.g., Li et al., 2004; Chen et al., 2008; Meng et al., 2012). Eastern Guangdong is located at the tectonic junction between the interior and the coastal South China (Fig. 1; Xu and Yue, 1999; Liu et al., 2015c). The region contains voluminous felsic rocks of both the Jurassic and Cretaceous phase (Huang et al., 2013a; Qiu et al., 2017), as well as widespread occurrences of mafic dike swarms. An example of mafic dikes with similar ages (late Jurassic to early Cretaceous) and contrasting geochemical characteristics is present in eastern Guangdong, which provides a good opportunity to tackle the problem as mentioned above.

2. Geological background and samples

The South China Block is composed of the Yangtze Block in the northwest and the Cathaysia Block in the southeast (Fig. 1a). Eastern Guangdong is located in the southeastern part of the Cathaysia Block. Regional stratigraphy is dominated by sedimentary rocks of the Upper Triassic Xiaoping and Lower Jurassic Jinji formations, volcanic rocks of the Upper Jurassic Gaojiping Formation, and the red beds and tuffaceous clastic rocks of the Lower Cretaceous Guancaohu Formation (Fig. 2; Xu and Yue, 1999; Liu et al., 2015). NE- and NW-trending faults are the major structures in the region, among which the three NE-trending faults of Lianhuashan, Puning–Chaozhou and Huilai–Raoping controlled the emplacements of Mesozoic magmatic rocks (Fig. 2). Jurassic–Early Cretaceous intrusions are widespread in eastern Guangdong, and comprise mainly granodiorite, monzogranite, biotite granite, quartz porphyry, granite porphyry and mafic dikes. Coeval volcanic rocks are widely distributed inside fault-bounded volcanic basins such as the Early Cretaceous Guancaohu basin (Qiu et al., 2017). Recently-published ages of granitoids and volcanic rocks in the region defined two magmatic phases at 165–152 Ma and 145–132 Ma (Yan et al., 2018). The latter phase, in particular, was largely coeval with the regional Sn—W and Cu polymetallic ore formation (145–135 Ma; Yan et al., 2017, 2018; Yan et al., 2020).

In eastern Guangdong, mafic dikes are NW- and NE-trending and individual dike is 0.2 to 3 m thick. In this paper, 20 representative mafic

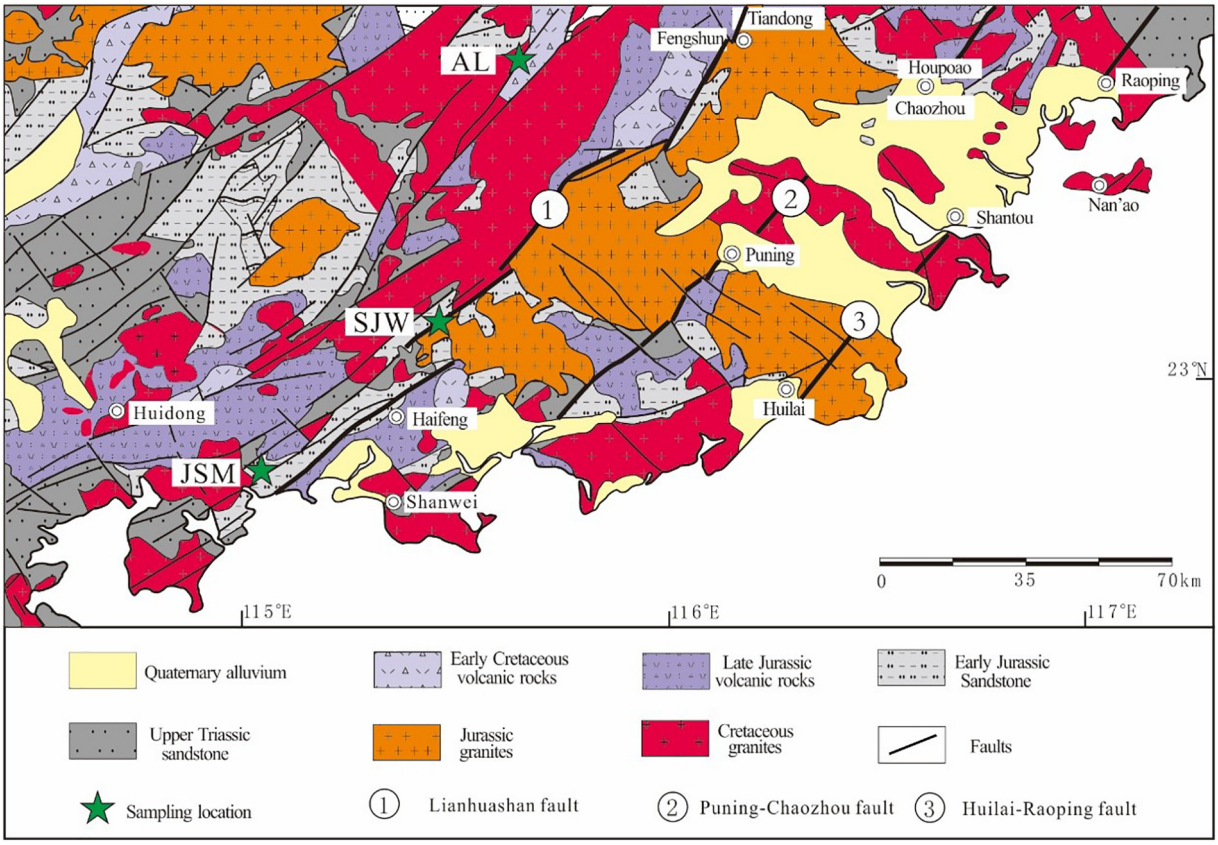

Fig. 2. Geologic map of eastern Guangdong (modified after Xu and Yue, 1999 and Liu et al., 2015a).

dike samples were collected near the Anliu (AL, n = 5), Sanjiaowo (SJW, n = 10) and Jishuimen (JSM, n = 5) areas. The AL and SJW dikes are lamprophyre, whilst the JSM dikes are dolerite (Fig. 3). The AL lamprophyre dikes intruded Mesozoic granitoids, and contain olivine, clinopyroxene, plagioclase and amphibole (Figs. 3a, b). Alteration minerals include carbonates, serpentine, and chlorite (Fig. 3b). The SJW lamprophyre dikes contain mainly plagioclase, amphibole and minor pyroxene (Fig. 3c–d). The phenocrysts (15–25 vol%) include dominantly euhedral amphibole, and the groundmass is composed of plagioclase, amphibole, magnetite and pyroxene. The JSM dolerite dikes are show ophitic texture, and contain dominantly clinopyroxene, plagioclase, olivine (mostly altered to iddingsite and minor to talc) and magnetite (Fig. 3e, f).

Mesozoic mafic dikes are newly found in the Eastern Guangdong (coastal South China) in this study (Fig. 3). A total of 20 mafic rock samples were collected, the analytical method and data are shown in the supporting information.

3. Methods

3.1. Zircon SIMS U—Pb dating

Zircons were separated using conventional heavy liquid and magnetic technique, handpicked under a binocular microscope, and then mounted in epoxy resin and polished to expose their cores. Cathodoluminescence (CL) imaging was conducted with a JXA-8100 Electron Probe Microanalyzer (EPMA) with a Mono CL3 CL system at the Guangzhou Institute of Geochemistry, Chinese Academy of Sciences (GIGCAS) to study the zircon internal structure, and to ensure the zircon grains are free of cracks or inclusions. Secondary ion mass spectrometry (SIMS) zircon U—Pb dating was performed with a CAMECA IMS1280-HR system at the State Key Laboratory of Isotope Geochronology, GIGCAS. Analytical procedures are similar to those described by Li et al. (2009). The Qinghu zircon (Li et al., 2013) was analyzed as a secondary standard to monitor the analysis reliability. Six analyses of the Qinghu zircon throughout the course of this study yielded a concordia age of 160.4 ± 2.9 Ma, consistent with its recommended value. Uncertainties on single analyses are reported at 1 σ level, whilst the mean ages for pooled U—Pb analyses are quoted at 95% confidence interval. Data reduction was performed with the software Isoplot/Ex 3 (Ludwig, 2003).

3.2. Whole-rock geochemical analyses

Whole-rock major and trace element contents were measured at the State Key Laboratory of Isotope Geochronology (GIGCAS). Major element concentrations (wt%) were determined with the fused glass technique, using a Rigaku ZSX100e X-Ray Fluorescence (XRF) spectrometer with accuracies of around 1% for SiO_2, 5% for MnO and P_2O_5, and 2% for other major elements. Trace element concentrations were measured with a Perkin-Elmer Sciex ELAN 6000 Inductively Coupled Plasma–Mass Spectrometry (ICP–MS) at GIGCAS, following the procedures described by Li et al. (2002). Analytical precision is generally better than 5% (Li et al., 2002).

3.3. In-situ Sr isotope analyses on plagioclase

In-situ Sr isotope analyses in this study were performed on a Neptune Plus MC-ICP-MS (Thermo Scientific), coupled with a RESOlution M-50193 nm laser ablation system (Resonetics), hosted at GIG-CAS. The laser parameters were set as follow: beam diameter, 112-155 μm; repetition rate, 6 Hz; energy density, ~4 J/cm^2. Each analysis consisted of 250 cycles with an integration time of 0.262 s per cycle. The first 30 s was used to detect the gas blank with the laser beam off, followed

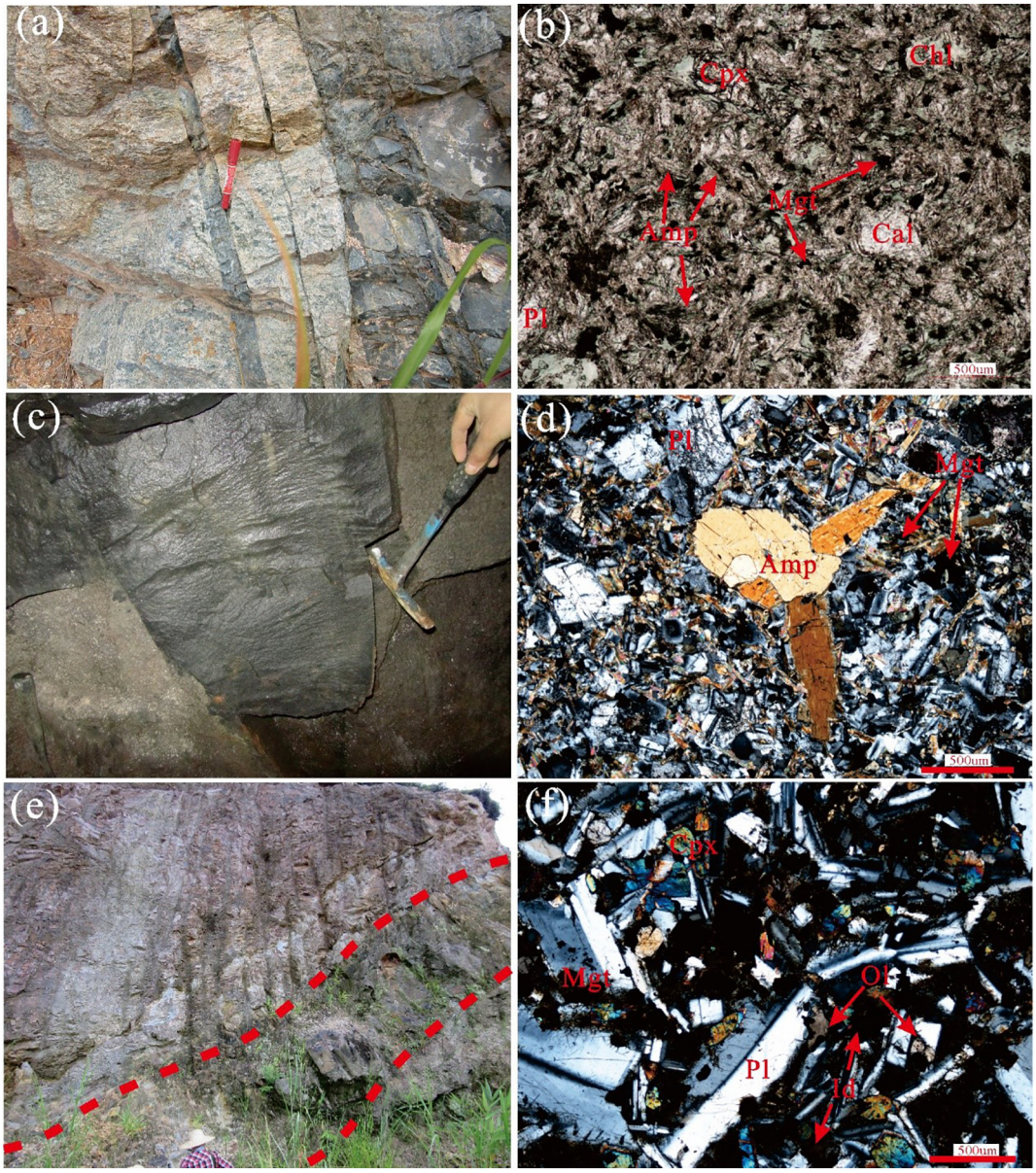

Fig. 3. Field occurrence and photomicrographs of mafic dikes in eastern Guangdong. (a) AL lamprophyre dikes intruded Mesozoic granite; (b) typical lamprophyric texture of AL dike. Many igneous minerals were altered to serpentine, chlorite and carbonates; (c) SJW lamprophyre dikes intruded granite at SJW Sn mine, (d) typical lamprophyric texture of SJW dike; (e) JSM dolerite dikes intruded sedimentary rocks of the Jinji Formation; (f) typical ophitic texture of JSM dolerite; Ol = olivine, Cpx = clinopyroxene, Pl = plagioclase, Id = iddingsite, Amp = amphibolite, Chl = chlorite, Cal = calcite.

by 30 s laser ablation for sample signals collection with laser beam on. During the measurement of this study, the gas blank of 83Kr and 88Sr were less than 2.5 mv and 0.5 mv. The interferences of ^{84}Kr and ^{86}Kr on ^{84}Sr and ^{86}Sr were corrected by subtracting gas blank from the raw time-resolved signal intensities. ^{85}Rb was used to correct the interference of ^{87}Rb on ^{87}Sr with a natural $^{85}Rb/^{87}Rb = 2.593$ (Catanzaro et al., 1969). The mass bias of $^{87}Sr/^{86}Sr$ was normalized to $^{86}Sr/^{88}Sr = 0.1194$ with an exponential law. The detailed data reduction procedure is reported in Zhang et al. (2018). Repeated analyses of the external standard NKT-1G yielded a weighted mean of $^{87}Sr/^{86}Sr = 0.70353 \pm 0.00009$ (2SD), which is consistent within error with the result reported value in Elburg et al. (2005).

3.4. Whole-rock Sr–Nd–Pb isotope analyses

For the analysis, the powdered samples were first dissolved in mixed HF + HNO_3 acid inside Teflon bombs, and then Sr and REEs were separated in cation columns. Detailed sample preparation and chemical separation procedures were similar to those outlined by Wei et al. (2002). Ratios of Sr—Nd isotopes were measured with a VG-354 Multi-Collector Inductively Coupled Plasma Mass Spectrometry (MC–ICP–MS) at GIGCAS, with the analytical procedures following those of Liang et al. (2003). Mass fractionation corrections of the Sr and Nd isotope ratios used $^{86}Sr/^{88}Sr = 0.1194$ and $^{156}Nd/^{144}Nd = 0.7219$, respectively. The NBS987 and Shin Etsu JNdi-1 were used as the standards, which yielded $^{87}Sr/^{86}Sr = 0.710237 \pm 9$ (2σ) and $^{143}Nd/^{144}Nd = 0.512097 \pm 4$ (2σ), respectively. Lead was separated and purified with the conventional cation-exchange technique, using dilute HBr as an eluant. Repeated analyses of NBS 981 yielded an average $^{206}Pb/^{204}Pb = 16.933 \pm 4$ (2σ), $^{207}Pb/^{204}Pb = 15.486 \pm 5$ (2σ) and $^{208}Pb/^{204}Pb = 36.682 \pm 2$ (2σ). The measured Sr (NBS 987), Nd (Shin Etsu JNdi-1) and Pb (NBS 981) isotope standards agree with recommended values reported by Zhang and Hu (2020) within uncertainty (Table S6).

4. Results

4.1. Zircon U—Pb geochronology

Zircon grains from 3 mafic dike suits are subhedral or anhedral, 40 and 100 μm long (aspect ratios = 1:1 to 2:1). They are translucent, and brown to purple. Under CL imaging, some zircon grains display weak oscillatory growth zoning, and some others are weakly zoned and/or have thin bright growth rims (Fig. 4a–c).

For the AL lamprophyre dike sample, 10 analyses yielded Th and U contents of 180–633 ppm and 229–1379 ppm, respectively. The Th/U ratios (0.37 to 0.84) are high and suggest a magmatic origin for the zircon grains (Table S1). The analysis gave a weighted mean $^{206}Pb/^{238}U$ age of 154.3 ± 3.4 Ma (Fig. 4d), which is interpreted as the crystallization age of the lamprophyre.

For the two SJW lamprophyre dike samples, zircon grains from sample SJW–1 (n = 7) and SJW–2 (n = 11) yielded Th (392–812 ppm and 105–635 ppm, respectively) and U (706–1821 ppm and 376–1416 ppm, respectively). Both samples display high Th/U ratios (0.26–0.56 and 0.23–0.92, respectively), suggesting a magmatic origin (Table S1). The samples SJW–1 and SJW–2 gave a weighted mean $^{206}Pb/^{238}U$ age of 141.3 ± 4.0 Ma and 143.2 ± 2.3 Ma, respectively (Fig. 4e–f).

For the JSM dolerite dike sample, 8 zircon grains yielded Th and U contents of 71–559 ppm and 189–863 ppm, respectively. The high Th/U ratios (0.38–0.65) indicate a magmatic origin (Table S1). The sample gave a weighted mean $^{206}Pb/^{238}U$ age of 141.7 ± 3.2 Ma (Fig. 4g).

4.2. Major and trace elements

The AL samples have relatively evolved compositions (Mg# = 53.7–58.1) and display narrow ranges of SiO_2 (48.42–50.57 wt%), Al_2O_3 (15.76–16.23 wt%), MgO (6.61–7.07 wt%), $Fe_2O_3^t$ (11.43–13.71 wt%), TiO_2 (1.04–1.09 wt%), CaO (3.13–5.58 wt%), Na_2O (1.09–1.49 wt%) and K_2O (1.37–2.34 wt%) (Table S2). Comparatively, the SJW samples have more primitive compositions (Mg# = 61.9.2–72.4, mean = 68.7) and contain higher SiO_2 (48.97–52.14 wt%), MgO (6.27–10.20 wt%), CaO (6.70–8.46 wt%), and Na_2O (1.94–3.38 wt%), lower Al_2O_3 (14.40–15.94 wt%), $Fe_2O_3^t$ (7.75–9.12 wt%) and TiO_2 (0.80–1.18 wt%) contents. The JSM samples contain lower MgO (3.77–5.04 wt%), Mg# (35.6–43.8), Cr (28.4–55.1 ppm) and Ni (37.2–71.1 ppm) contents than their AL and SJW counterparts, but have higher $Fe_2O_3^t$ (14.89–15.82 wt%) and TiO_2 (2.88–3.06 wt%). In the Nb/Y-Zr/TiO2 diagram (Fig. 5), the samples fall into the andesite and the alkaline fields.

For trace elements, the AL and SJW samples have much higher Cr (206.8–343.2 ppm and 100.9–780.2 ppm, respectively) and Ni (94.6–124.7 ppm and 40.2–261.0 ppm) contents than those from JSM

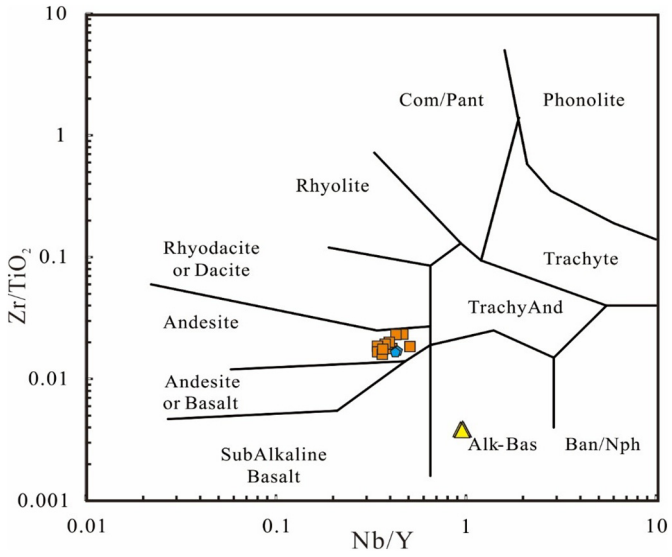

Fig. 5. Nb/Y-Zr/TiO_2 diagram (after Winchester and Floyd, 1977) for mafic dikes in eastern Guangdong.

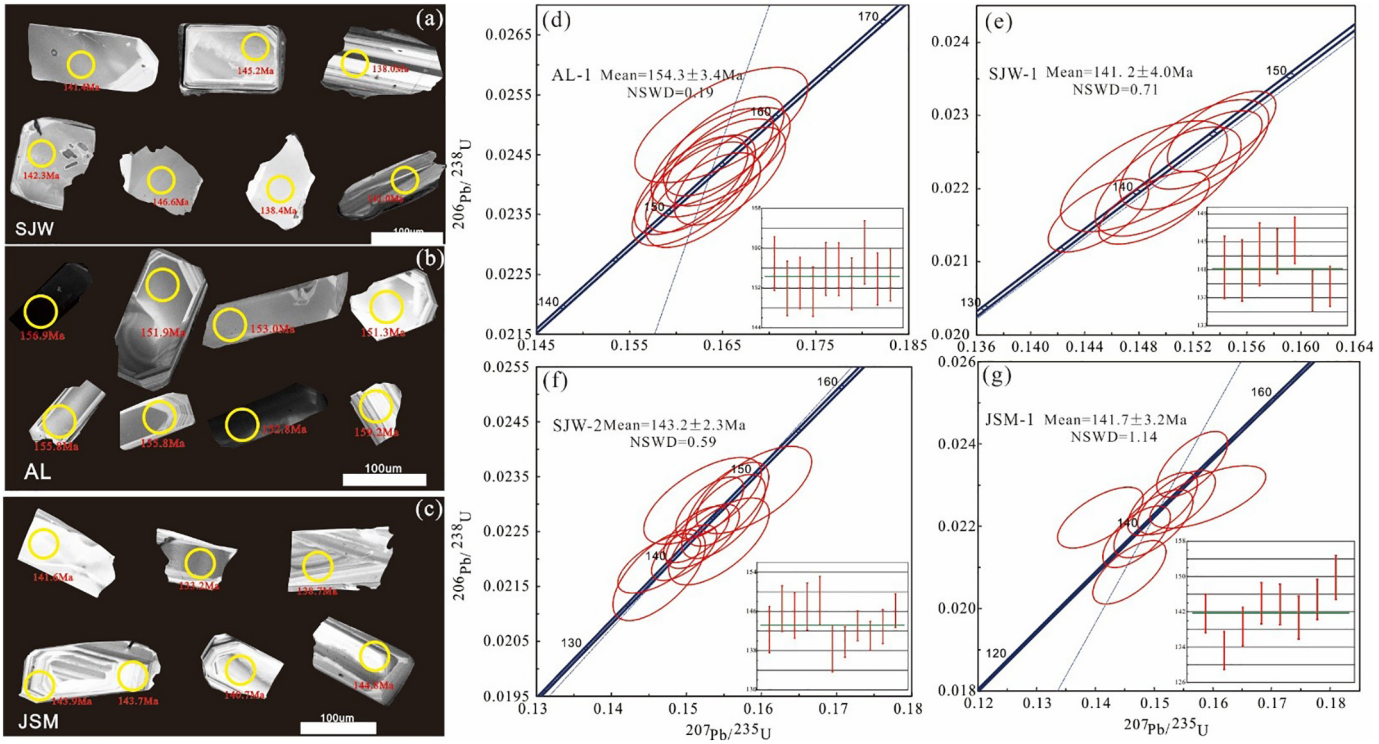

Fig. 4. CL images (a–c) and SIMS zircon U—Pb concordia diagrams (d–g) of representative zircon grains from AL, SJW, and JSM mafic dike samples.

(Cr = 28.4–55.1 ppm and Ni = 37.2–71.1 ppm). In the chondrite-normalized REE diagram (Fig. 6), all the mafic dike samples share similar high total REE contents (∑REE = 240.0–248.0, 118.2–374.4, and 149.9–259.8 ppm for AL, SJW and JSM, respectively), light REE (LREE) enrichments, and strong LREE/HREE fractionation ($(La/Yb)_N$ = 17.7–19.9, 9.4–33.4, and 7.0–8.7 for AL, SJW and JSM, respectively). All the samples display slight negative Eu anomalies. In the primitive mantle (PM)-normalized multi-element spider diagram (Fig. 6a, c, and e), the AL and SJW samples show distinct negative Nb, Ta, Zr, Hf and Ti anomalies, resembling arc-type magmas (Fig. 6b, d). In contrast, the JSM samples show convex PM-normalized multi-element patterns. They display enrichments in LILEs (e.g., Rb and U) and HFSEs (e.g., Nb and Ta), which mimics typical alkali ocean island basalt (OIB) (Sun and McDonough, 1989) except for the slight Sr—Ti depletions (Fig. 6f).

4.3. In-situ Sr isotopes of plagioclase

In-situ Sr isotopes of plagioclase are listed in Appended Table S3. To be specific, a total of eight Sr isotope analyses on plagioclase from the AL yield a range from 0.706173 to 0.711984. Ten Sr isotope analyses on plagioclase grains from the SJW show an $^{87}Sr/^{86}Sr$ range from 0.705728 to 0.706649. Fourteen Sr isotope analyses on plagioclase from the JSM give an $^{87}Sr/^{86}Sr$ range from 0.704886 to 0.705361. Generally, the measured Sr isotope ratios within a single plagioclase crystal and among different plagioclase crystals from SJW and JSM dikes (all the plagioclase crystal are fresh) are similar or even identical to the whole-rock Sr isotope ratios from each intrusion. However, large variation of Sr isotope ratios in plagioclase are observed in the AL dikes. The relatively fresh grains possess low $^{87}Sr/^{86}Sr_i$ (0.706173 to 0.706361) similar to those from the SJW dikes, whereas the altered ones have increasingly higher $^{87}Sr/^{86}Sr_i$ (Fig. 7).

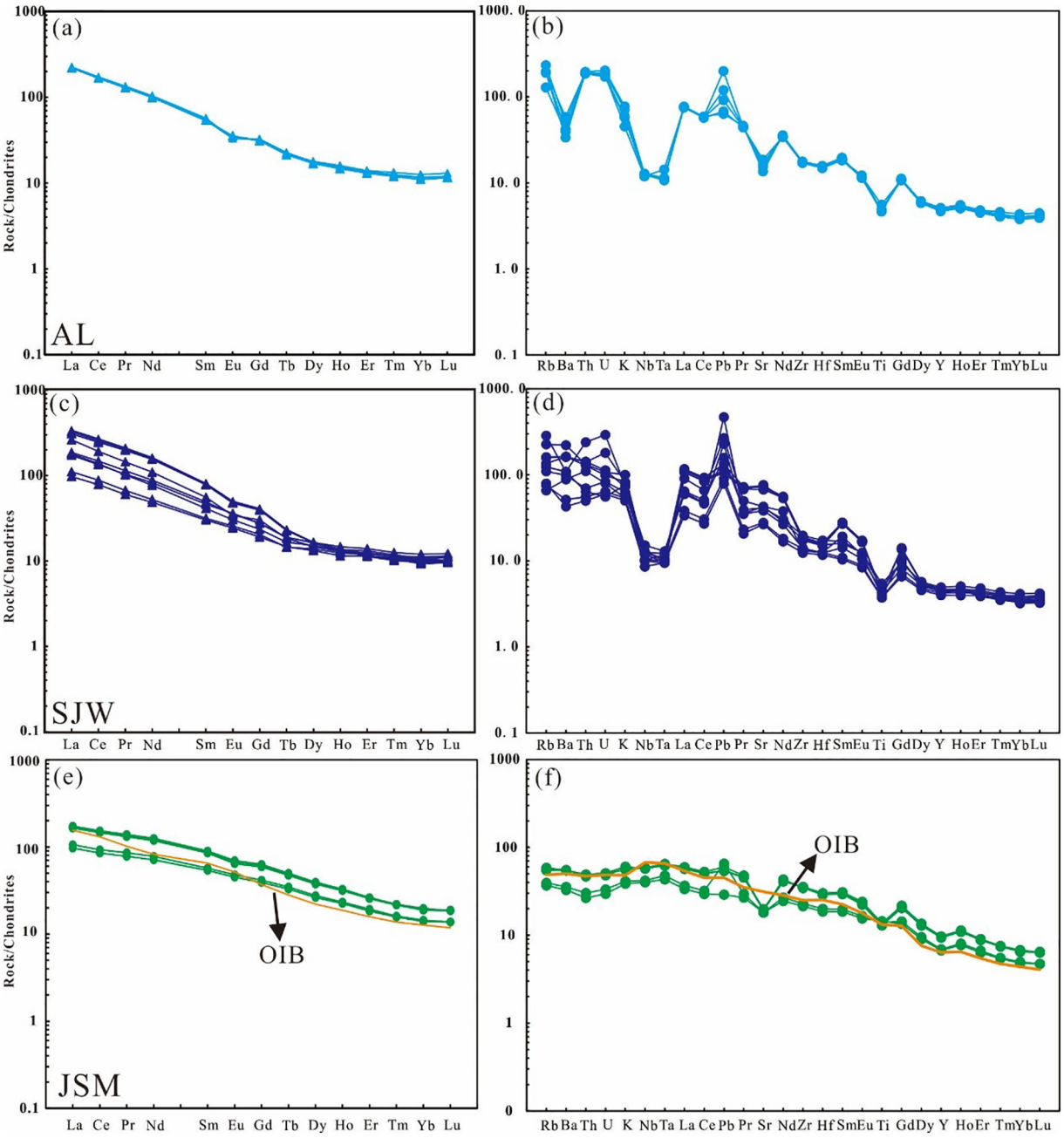

Fig. 6. Chondrite-normalized REE (a, c and e) and primitive-mantle-normalized multi-element diagrams (b, d and f) for mafic dikes in eastern Guangdong (normalizing values are from Sun and McDonough, 1989).

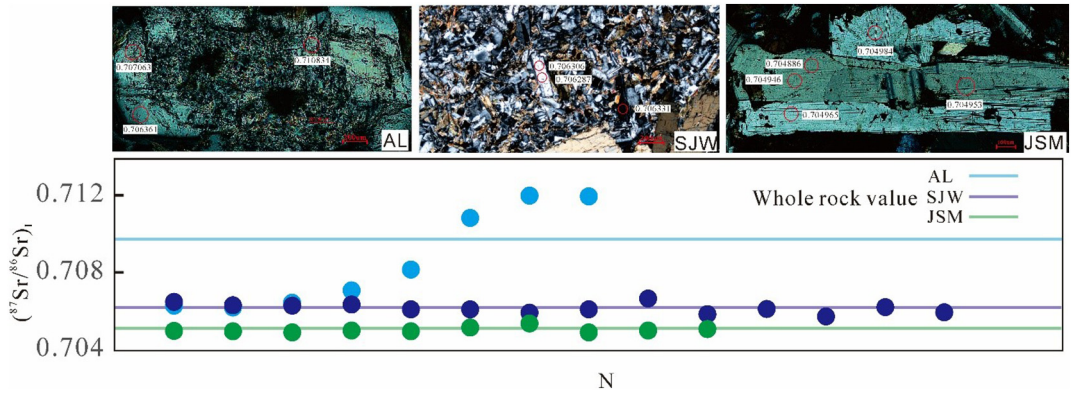

Fig. 7. In-situ analysis of Sr isotopes in plagioclase from the mafic dikes in eastern Guangdong.

4.4. Whole-rock Sr–Nd–Pb isotopes

Whole-rock S–Nd–Pb isotope data are present in Table S4. The initial $^{87}Sr/^{86}Sr$ and $\varepsilon_{Nd}(t)$ values are calculated based on the zircon U—Pb ages, i.e., 154 Ma for AL, 142 Ma for SJW and 141 Ma for JSM. The calculated initial $^{87}Sr/^{86}Sr$ values of AL fall into a narrow range (0.709633 to 0.710133) (Table S4). Their $\varepsilon_{Nd}(t)$ range from −1.68 to −1.42, with corresponding TDM_2 of 1058–1079 Ma. The initial whole-rock $^{206}Pb/^{204}Pb_i$, $^{207}Pb/^{204}Pb_i$ and $^{208}Pb/^{204}Pb_i$ values are 17.821–18.217, 15.626–15.644 and 38.032–38.395, respectively (Table S4). The SJW samples have calculated initial $^{87}Sr/^{86}Sr$ values of 0.705682 to 0.706945 (Table S4) and $\varepsilon_{Nd}(t)$ values of −4.49 to −1.49, with corresponding TDM_2 of 1054–1298 Ma. The whole-rock $^{206}Pb/^{204}Pb_i$, $^{207}Pb/^{204}Pb_i$ and $^{208}Pb/^{204}Pb_i$ values are 18.405–18.695, 15.628–15.652 and 38.443–39.051, respectively (Table S5). Initial $\varepsilon_{Nd}(t)$ and $^{86}Sr/^{87}Sr$ values of the JSM samples range from +3.63 to +4.25 and 0.704999 to 0.705398, respectively. The whole-rock $^{206}Pb/^{204}Pb_i$, $^{207}Pb/^{204}Pb_i$ and $^{208}Pb/^{204}Pb_i$ values are of 18.329–18.445, 15.625–15.630 and 38.483–38.605, respectively (Table S5).

5. Discussion

5.1. Assessment of alteration, crustal contamination and magma differentiation

We note that samples used in this study have variably high LOI values (1.81–6.82%), especially the AL dikes (LOI = 5.67–6.82%), suggesting the samples experienced various degrees of alteration. Zirconium is usually used to assess the geochemical mobility of other elements due to its immobile feature (e.g., Polat et al., 2002). For the AL dike samples, high LOI and quite a number of altered minerals (e.g., chlorite and calcite) indicate high degree of alteration of these samples, which is consistent with the scattering distribution of Na, K, Ca, Rb, Mn and Al vs. Zr. Chemical weathering processes can significantly change $^{87}Sr/^{86}Sr$ ratios, indicating the high $^{87}Sr/^{86}Sr$ ratios of AL dikes (Table S4) may be caused by alteration. This is consistent with the large variation of Sr isotope ratios in plagioclase with relatively fresh grains possess low $^{87}Sr/^{86}Sr$ and alterated ones have increasingly higher $^{87}Sr/^{86}Sr$ (Fig. 7).Whereas, HFSEs, Y, Th, U, and Ba still show linear correlation with Zr, indicating that these elements are essentially immobile. For the SJW dikes, good correlation of Zr with HFSEs, Y, Sr, La, Ba, Rb, Mn, K, Na, P, Fe, and Al indicate that these elements are essentially immobile. The JSM dike samples are generally fresh (LOI = 1.68–2.92) and the Zr content is well correlated with those of HFSEs, REEs and LILEs, indicating that these elements are essentially immobile.

In the primitive-mantle-normalized incompatible element patterns based on whole rock geochemistry, the JSM dikes show positive Nb and Ta anomalies (Fig. 6), indicating negligible crustal contamination because the continental crust is generally characterized by enrichments of LILEs and depletions of HFSEs (e.g., DePaolo, 1981; Gao et al., 1998). In addition, the Nb/U and Ce/Pb (except one: 15JSM-2) values of the JSM dike is similar to those of MORBs and OIBs (47 ± 10 and 25 ± 5, Hofmann et al., 1986), suggesting imperceptible contamination from the crust. In contrast, the negative Nb—Ta and positive Pb anomalies, enrichment of LILE and Nd isotope compositions of AL and SJW mafic dikes may be caused by crustal assimilation because continental crust has much higher LILEs, lower Nb—Ta contents and more enriched Sr—Nd isotopes than those in the mantle (e.g., Rudnick and Gao, 2003). However, magmas undergone crust contamination would exhibit positive Ce/Pb vs. MgO correlations, since crustal contamination, if any, might have decreased the Ce/Pb ratios. The lack of positive correlation between Ce/Pb versus MgO (Fig. 8), rules out the possibility of significant crustal contamination . This interpretation is further supported by almost the same $^{87}Sr/^{86}Sr$ ratios of the plagioclases (the fresh ones) in these samples.

The positive correlation between Mg# and Sc, Cr and Ni (Fig. 9 c–e) of the JSM dikes suggest probable fractionation of olivine and clinopyroxene. TiO_2 and δEu increase slightly with increasing Mg# (Fig. 9 b, f), suggesting minor fractionation of Fe—Ti oxides and plagioclase, which is also supported by the subtle negative anomalies of Sr and Ti. The positive correlation between Mg# and Sc, Cr and Ni (Fig. 9 c–e) of the SJW samples suggest probable fractionation of olivine and clinopyroxene. The decrease of CaO with decreasing MgO of the SJW and AL samples also indicates clinopyroxene fractionation (Fig. 9 a).

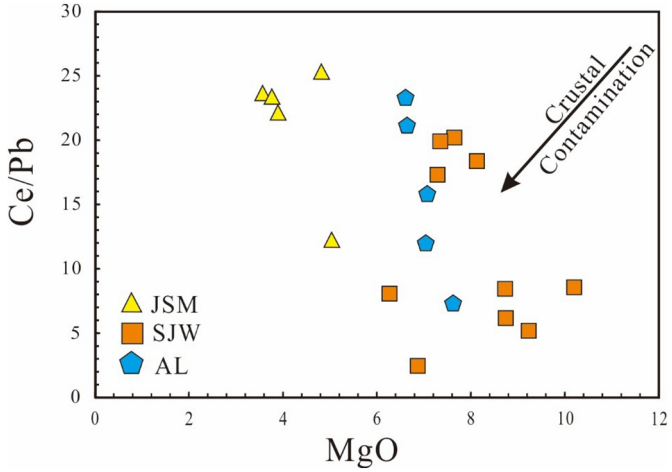

Fig. 8. Plots of Ce/Pb vs. MgO for mafic dikes in eastern Guangdong.

5.2. Magma source

5.2.1. SJW and AL Arc-like dikes: Metasomatized lithospheric mantle related to subduction

The AL and SJW mafic dikes show crustal-like trace element and isotopic features such as LREE and LILE enrichments and HFSE depletions, and negative $\varepsilon_{Nd}(t)$ values. Having precluded the effect of continental crustal contamination, this crustal-like feature of the mafic rocks may be derived from (1) an enriched lithospheric mantle that has been metamorphosed by fluids derived from the subducting slab; (2) an asthenospheric mantle source that has been contaminated by subducted sediments. However, the following evidence indicate that the mantle source of SJW and AL Arc-like dikes should be metasomatized lithospheric mantle rather than sediment-bearing asthenosphere: (1) subducted sediments are generally rich in Ba and have a high Ba/Th ratio (Plank, 2014). The depleted mantle reservoir contaminated by subducted sediments would have high Ba/Th ratio (~150–250, e.g., Liu et al., 2015b; Chen et al., 2017), which is inconsistent with the relatively low Ba/Th ratio of SJW and AL dikes (AL: average = 19.3; SJW: average = 93.6, Fig. 6); (2) the relative low $^{87}Sr/^{86}Sr$ ratios of SJW dikes are inconsistent with the binary mixing between asthenosphere and subducted sediments (Fig. 9). For the AL dikes, although it seems that subducted sediments mixture could account for the whole-rock Sr—Nd isotopic compositions of AL samples (Fig. 10), considering the high LOI (5.67–6.82%) and existence of quite a number of chlorite and calcite in these samples (Fig. 3b), it is reasonable to speculate that high whole-rock Sr isotopes of AL dikes were possibly caused by later chemical weathering processes and their original values may most likely represented by the in-situ plagioclase Sr isotope compositions (the fresh grains), which are also deviation from mixing line (Fig. 9). Furthermore, the AL and SJW dikes formed in relatively lower depth than the asthenospheric derived JSM dikes (see below), indicating a possible lithospheric mantle source; (3) the near-primary SJW dikes have geochemical characteristics of relative high SiO_2 (49.0–52.1 wt%), Mg# (66.0–72.4), Cr(100.9–780.2 ppm, Average = 371.9 ppm) and Ni (40–261 ppm, Average = 167.7 ppm), which are much

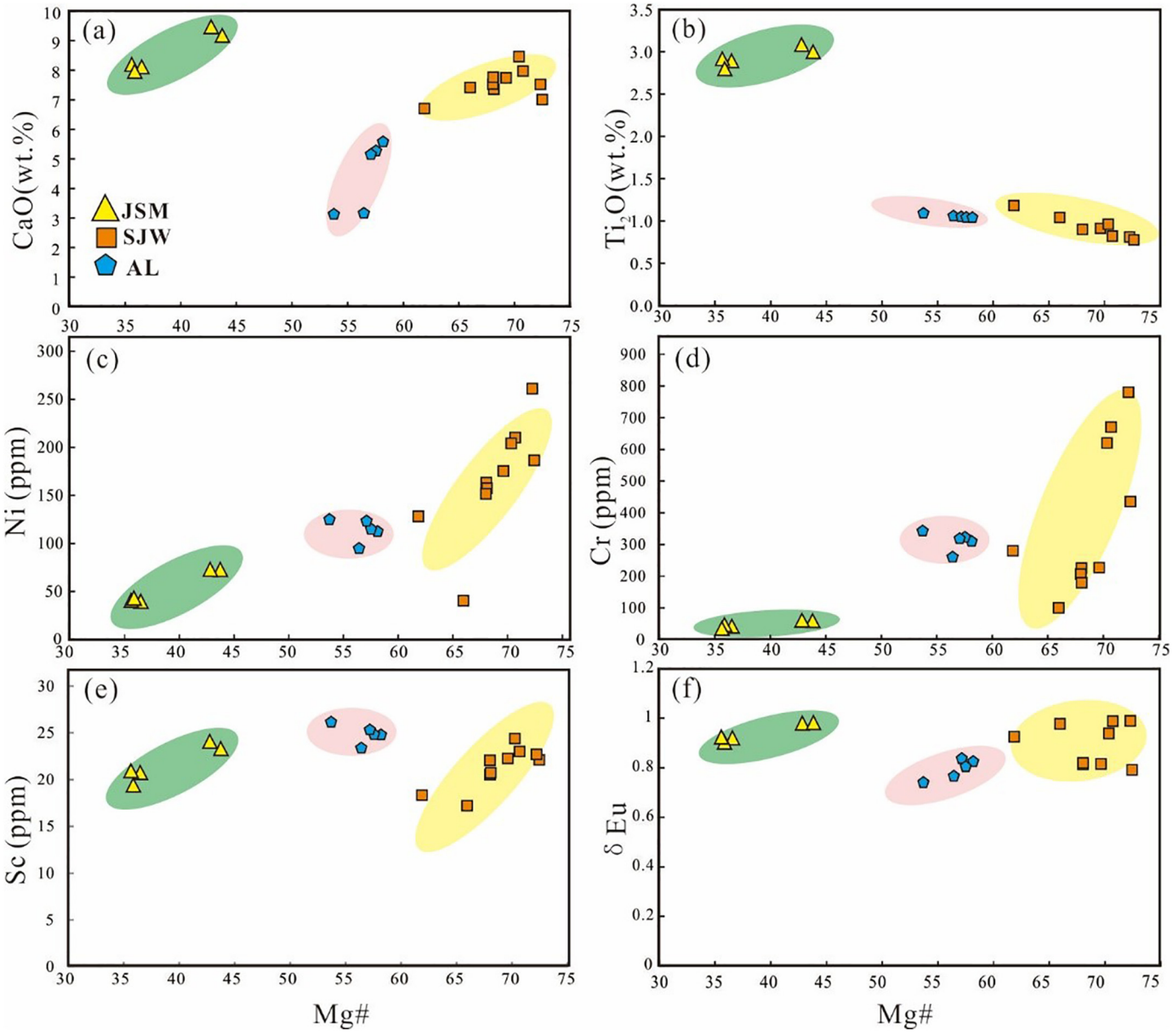

Fig. 9. Binary plots of major oxides and trace elements vs. Mg# for the mafic dikes in eastern Guangdong.

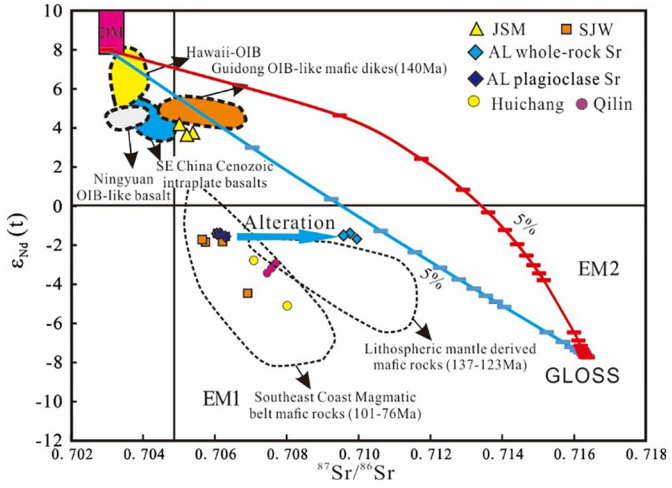

Fig. 10. $^{87}Sr/^{86}Sr_i$ vs. $\varepsilon_{Nd}(t)$ diagrams for Mesozoic mafic dikes in eastern Guangdong. Data sources: The Qilin Arc-like basalt (Huang et al., 2013b); the Huichang and SE China Coastal Magmatic Belt Arc-like basalts (Chen et al., 2008); the Ningyuan OIB-like basalt (Li et al., 2004); the Guidong OIB-like mafic dikes (Li and McCulloch, 1998); The mixing end-members are: Global subducting sediment (GLOSS) from Plank and Langmuir (1998) and Ma et al., (2017) and DMM form Workman and Hart (2005). The red line represent mixture of DMM and Gloss melt and the green line represents mixture of DMM and Gloss.

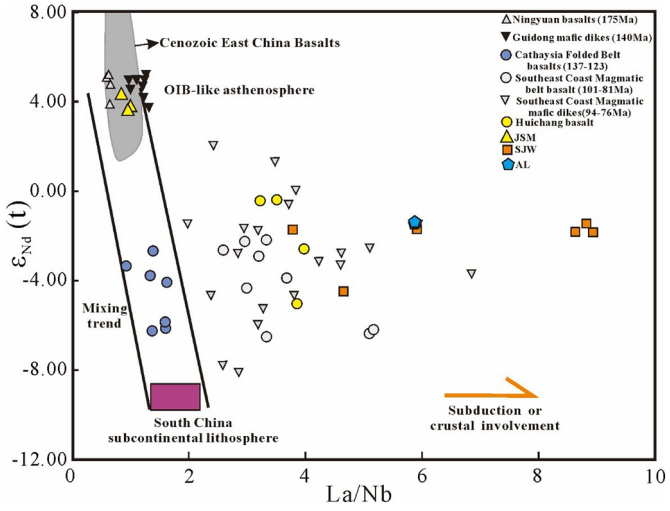

Fig. 11. Plot of La/Nb vs. $\varepsilon_{Nd}(t)$ of Mesozoic basalts from South China. The OIB-asthenosphere and South China SCLM (subcontinental lithosphere mantle) components are after Chen et al. (2008). Data are from Chen et al. (2008) and references therein.

close to high-Mg andesite and could be derived from partial melting of hydrous lithospheric mantle (Ma et al., 2017); (4) the mafic dikes in this study have trace element and isotopic signatures different from those derived from binary mixing between asthenosphere and subducted sediments (e.g., generally with depleted Nd isotopes and without negative Nb—Ta anomalies; Liu et al., 2015a, 2017; Chen et al., 2015, 2017; Xia et al., 2015) but similar to the mafic rocks in South China Coastal Magmatic Belt (101–76 Ma) (Chen et al., 2008; Fig. 10), which were generally considered to be derived from subduction-related enriched subcontinental lithosphere mantle (SCLM) (e.g., Xie et al., 2001; Chen et al., 2008). Moreover, trace element ratios (e.g., La/Nb) and Sr—Nd isotopic compositions are considered to be magma source-related and can thus reflect source variation, such as the relative contribution from crustal contamination and subduction (e.g., Chen et al., 2008; De Paolo and Daley's, 2000). The high La/Nb and low ε_{Nd} (T) ratios of SJW and AL samples are much close to the Southeast Coast Magmatic Belt basalts and mafic dikes (Fig. 11), further suggesting a subduction-related enriched SCLM source.

The composition of the mantle source and degree of partial melting that produced the precursor magmas of the gabbroic and the doleritic dykes can be constrained by REE abundances and ratios. Sm and Yb have similar partition coefficients during partial melting of a spinel lherzolite mantle source, thus the Sm/Yb ratio does not change during the partial melting, whereas, the La/Sm ratio decrease during partial melting process (Aldanmaz et al., 2000). Therefore, partial melting of a spinel lherzolite source will define clear trends in Sm/Yb versus La/Sm diagrams (Zhao and Zhou, 2007). In contrast, partial melting of garnet lherzolite mantle with residual garnet will produce a more steep-slope trend on a Sm/ Yb versus La/Sm because garnet has a high partition coefficient for Yb ($D_{garnet/melt} = 6.6$) relative to Sm ($D_{garnet/melt} = 0.25$) (Johnson, 1994). A plot of Sm/Yb vs. La/Sm diagram (Fig. 13) is used here to constrain their source characteristics and the degree of partial melting (Aldanmaz et al., 2000; Zhao and Zhou, 2007). The results show that the SJW dikes plot between the partial melting curves of garnet-facies lherzolite and garnet + spinel lherzolite-facies lherzolite, reflecting low but varying extents of partial melting in the garnet-stability to spinel-garnet transition mantle source, which is inferred to be at the bottom of the continental lithosphere mantle (Fig. 13). The AL mafic dikes all plot near the garnet + spinel lherzolite mantle source (Fig. 13). Therefore, we suggest that the SJW and AL arc-like dikes could be derived from partial melting of a metasomatized lithospheric mantle related to the subduction of Paleo-Pacific slab.

5.2.2. JSM OIB-like dikes: asthenospheric mantle source

Compared to the AL and SJW dikes, the JSM alkaline mafic dikes (ca. 141 Ma) have lower SiO_2, more depleted Nd isotopes, and higher TiO_2 contents. The JSM dikes possess no HFSE depletions and exhibit PM-normalized OIB-like multi-element characteristics (Figs. 6e-f) (e.g., Sun and McDonough, 1989). The OIB-like features are manifested by the Nb/La (1.02–1.24), Nb/U (39.7–46.4), Th/La (0.10–0.11) and Th/Ta (1.28–1.64) values, which are clearly different from those of N-MORB or arc-type volcanics (e.g., Sun and McDonough, 1989). The JSM mafic dikes have high contents of incompatible trace elements (Fig. 6f), which indicates an enriched magma source. This is further supported by the elevated Ta/Yb ratios, with the JSM data falling inside the enriched mantle field (Fig. 13). These features are similar to many continental alkaline magmatic suites that have positive $\varepsilon_{Nd}(t)$, and no Nb—Ta anomalies in association with LREE enrichments, which suggest an OIB-like asthenospheric mantle source (e.g., coeval Guidong OIB-like mafic dikes; Li and McCulloch, 1998; Cenozoic South China intraplate basalts; Huang et al., 2013b; Tu et al., 1992; Late Cenozoic intraplate alkali basalts in the Lut–Sistan region; Pang et al., 2012). The presence of asthenospheric mantle source is further supported by their relatively high $\varepsilon_{Nd}(t)$ (2.61 to 3.32) and low La/Nb (0.80 to 0.98) values, which fall into the asthenosphere-origin field (Fig. 12).

Positive $\varepsilon_{Nd}(t)$, alkalis coupled with incompatible trace elements including LREE enrichment indicate that OIB-like mantle source has experienced an ancient melt-removal event (shown by the depleted radiogenic isotopic compositions), and then refertilized by metasomatism (which was too young to produce a time-integrated change in radiogenic isotopic ratios). This refertilization event has often been attributed to the addition of oceanic sediments during subduction (Hofmann and White, 1982; Chauvel et al., 1992). Alternatively, the enriched components could enter the mantle by metasomatism (Sun and McDonough, 1989; Niu and O'Hara, 2003), through (1) incorporation of small volume of melts or subduction-related fluids from the lithospheric mantle (McKenzie, 1989; Anderson, 1994) during passage of asthenosphere-derived magmas, and (2) migration of volatile-rich fluids or melts released from the subsolidus peridotite shortly before the melting (Zou and Zindler, 1996) or from the low-velocity zone in

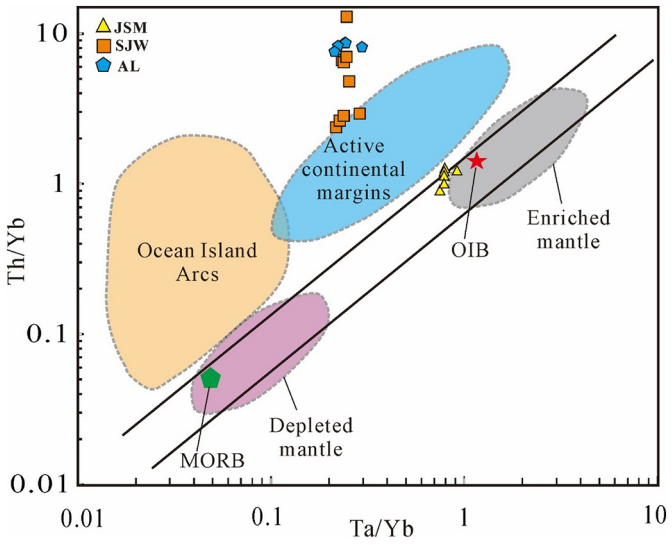

Fig. 12. Ta/Yb vs. Th/Yb diagram (after Orejana et al., 2008) for mafic dikes in eastern Guangdong.

the asthenosphere (Niu, 2008). The latter was more likely due to the lack of arc-related geochemical features (e.g. Nb—Ta anomalies) of the alkali basalts as above-mentioned. In the Sm/Yb vs. La/Sm diagram (Fig. 13), the JSM mafic dikes fall in the garnet- peridotite zone (Fig. 13), indicating they may originated from garnet-stability zone in the mantle, which is deeper than the SJW and AL dikes.

5.3. Mantle dynamics and deep-seated process

5.3.1. Jurassic Subduction of Paleo-Pacific plate

Early Yanshanian magmatism (bimodal volcanic rocks, alkaline rocks and I- and A-type granites) in South China mainly occurred during ca. 155 to 190 Ma in the interior areas (Zhou et al., 2006; Li and Li, 2007). This magmatism event began with the eruptions of Xialan intraplate basalt (196 Ma) and peaked at 175–155 Ma, after the magmatic

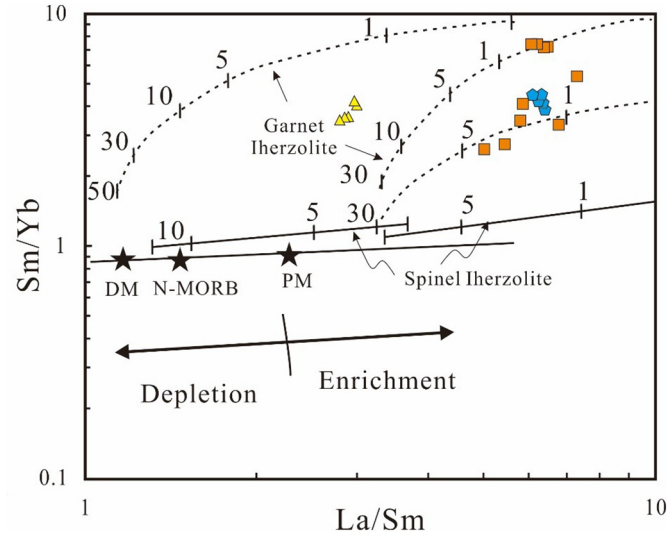

Fig. 13. Plots of La/Sm vs. Sm/Yb (b) (Zhao and Zhou, 2007) for the mafic dikes in eastern Guangdong. Mantle array (heavy line) defined by depleted MORB mantle (DMM, McKenzie and O'Nions, 1991) and primitive mantle (PM, Sun and McDonough, 1989). Melting curves for spinel lherzolite (Ol_{53} + Opx_{27} + Cpx_{17} + Sp_{11}) and garnet peridotite (Ol_{60} + Opx_{20} + Cpx_{10} + Gt_{10}) with both DMM and PM compositions are after Aldanmaz et al. (2000). Numbers along lines represent the degree of the partial melting.

quiescence during the late Triassic to Early Jurassic boundary (Li et al., 2004; Zhou et al., 2006). However, despite decades of research, it is still debated on whether these Early Yanshanian magmatism are associated with the Pacific subduction (e.g., Jahn et al., 1990; Zhou and Li, 2000; Li and Li, 2007; Chen et al., 2008; Gan et al., 2018).

In this study, geochemical and isotopic data indicate that the Early Yanshanian AL arc-like mafic dikes were derived from the subduction-fluid metasomatic lithospheric mantle, suggesting the influence of Paleo-Pacific subduction. This is further supported by the elevated Th/Yb ratios that fall inside the active continental margin field (Fig. 12). All these argues against the post-orogenic and the intraplate extension models, and suggest the Early Yanshanian subduction in South China. This is further supported by the slightly subducted-fluid influenced asthenosphere origin of the middle Jurassic Changchengling and Ningyuan basaltic rocks (Jiang et al., 2009).

Despite of the disagreement of the specific subduction pattern, it is noted that the generally accepted tectonics during early Yanshanian (Jurassic) in the interior South China is extension, as represented by extensive distributed intraplate A-type granites, bimodal magmatism, mafic rocks (dikes and basalts) and concentrated granitoids and related W—Sn mineralization (mainly 165–150 Ma) in the interior areas (e.g., Chen et al., 2008; Jiang et al., 2009; Li and Li, 2007; Mao et al., 2013). The extension thus excludes the normal Paleo-Pacific subduction (e.g., Jahn et al., 1990). Hence, the subducted related models responsible for extensional tectonics in South China may be low-angle subduction model with changing subduction angles, namely slab-rollback (Zhou and Li, 2000), foundering of a flat-slab subduction (Li and Li, 2007), and slab tearing or window opening within the subducting Plate (Mao et al., 2013). In recent years, extensive Early Yanshanian magmatism (mainly 165–152 Ma) has also been documented in the coastal area, which is also interpreted to have formed in an extensional setting (e, g., Guo et al., 2012; Huang et al., 2013a; Qiu et al., 2017), indicating extensional tectonics occurred within a huge areas from the continental interior to coastal areas (ca. 600 km) during this time. The extensive extensional tectonic setting thus may rule out the slab rollback and the slab tearing models, because the slab rollback (back-arc extension) and slab window opening are unlikely to have an influence on such a huge areas (inducing such huge essentially simultaneous magmatism from the continental interior to coastal areas). Consequently, the flat-slab model, which ascribed the generation of early Yanshanian magmatism to "slab foundering" as a consequence of rollback of the retreating flat subduction (Li and Li, 2007) may provide the best explanation of the temporal–spatial geochemical variations demonstrated by the Mesozoic magmatism. Such a model can explain the extensively distributed but temporally concentrated early Yanshanian magmatism (including mafic and felsic rocks) and related deposits in South China. Furthermore, here we emphasize that the tectonic response to "slab foundering" has also occurred in the coastal area during late Jurassic. During the incipient slab-foundering, due to no or little dehydration due to the shallow depth, early to middle Jurassic intraplate mafic rocks in the interior areas such as Ningyuan, Antang and Chebu etc. (Fig. 1) show typical OIB-like geochemical compositions due to the melting of the upwelling asthenosphere, without distinguishable influx of suducted-related materials. However, when the flat-slab foundering became fully developed, the intensified dehydration of the sinking flat-slab at higher mantle temperatures (Peacock and Wang, 1999), induced the late Jurassic arc-like mafic dikes (Fig. 14a). Lithosphere thinning induced high-degree of partial melting of the continental lithospheric mantle and substantial basaltic underplating, which further induced the anatexis of the crustal rocks, producing the widespread granitoids and related W–Sn–Cu–Mo mineralization during Early Yanshanian in South China.

5.3.2. Initial slab roll-back and related deep process in early cretaceous

A short compressive event at the Jurassic–Cretaceous boundary representing by the magmatic quiescence, regional unconformity and

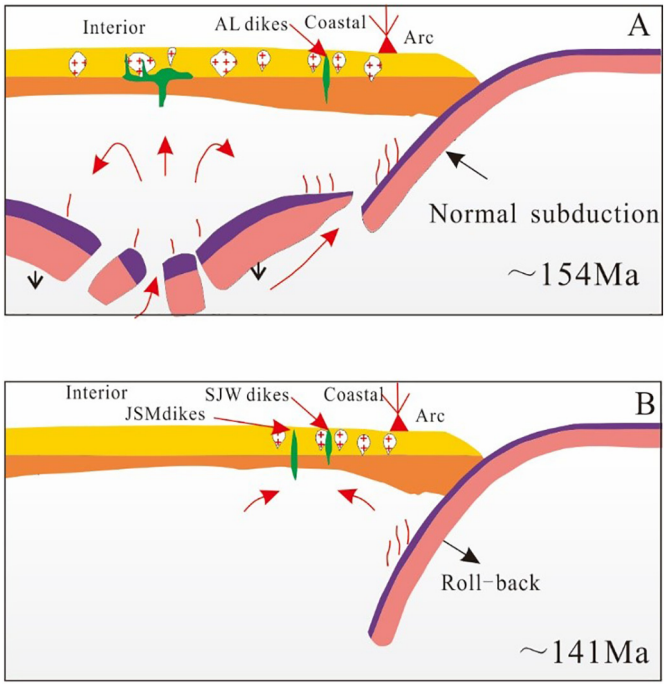

Fig. 14. Schematic geodynamic model for the formation of the (a) Late Jurassic (154 Ma) (b) Early Cretaceous (141 Ma) in coastal SE China (modified after Li and Li, 2007; Huang et al., 2013a).

weak mineralization across most of the South China Block has been reported by many researches (e.g., Gilder et al., 1991; Shu et al., 2009; Jiang et al., 2011). Soon afterwards, extensive A-type granite and the basin and range province occurred, demonstrating a dominant regional extension in South China in the Early Cretaceous (Gilder et al., 1991; Shu et al., 2009; Yang et al., 2012; Zhou et al., 2016). Different from the early Yanshanian stage, the Cretaceous voluminous felsic volcanism is generally interpreted to be related to Paleo-Pacific subduction and the extensional tectonics in the late Yanshanian is widely accepted to be caused by the Paleo-Pacific slab rollback (e.g., Wong et al., 2009; Zhou et al., 2016; Li and Li, 2017; Liu et al., 2015a). However, as mentioned above, the starting time of this transition and the deep processes associated with it are not well understood (e.g., Wong et al., 2009; Zhu et al., 2014; Liu et al., 2015a; Zhou et al., 2016; Yan et al., 2018).

Slab-rollback generally lead to the upwelling of the hot asthenosphere. Then, upwelling of asthenosphere consuming the lithospheric mantle by thermo-mechanical-chemical erosion, and/or lithospheric delamination caused the lithospheric thinning. Mantle thinning would lead to lithospheric extension and decompression melting of the asthenosphere, which gives rise to the OIB-like JSM mafic rocks (Fig. 14b). At the same time, the lithospheric mantle may have partially melted due to the heating by the upwelling asthenosphere to generate the simultaneous SJW Arc-like mafic dikes (Fig. 14b). The age of mantle thinning can provide a good constrain on the initiation of slab rollback and lithospheric extension. Therefore, the simultaneous arc-like SJW and OIB-like mafic dikes suggest that the initial slab rollback and corresponding back-arc extension occurred potentially before ca. 141 Ma.

6. Conclusions

(1) The mafic dikes in eastern Guangdong comprise lamprophyre and dolerite, and were emplaced in three episodes of ~154 Ma, ~141–143 Ma, and ~141 Ma.
(2) The AL and SJW dikes show typical arc-like features and were considered to be derived from partial melting of subcontinental lithospheric mantle metasomatized by the slab fluids from the Paleo-Pacific subduction.
(3) The occurrence of AL arc-type lamprophyre argues against the post-orogenic model, and reflects the oldest Paleo-Pacific subduction-related arc-type mafic rocks documented in South China.
(4) The JSM dikes exhibit typical OIB-type multi-element characteristics, and were derived from partial melting of asthenospheric mantle in the garnet-stability zone.
(5) The coeval SJW arc-like lamprophyre and JSM OIB-like dolerite suggest the initial roll-back of Paleo-Pacific plate occurred potentially before ca. 141 Ma.

Declaration of Competing Interest

We seriously declare that the submitted manuscript of "Simultaneous development of arc-like and OIB-like mafic dikes in eastern Guangdong, SE China: implications for late Jurassic – early Cretaceous tectonic setting and deep geodynamic processes of South China" written by Qing-He Yan, He Wang, Guoxiang Chi, and Yangming Wu to Lithos has no conflict of interest.

Acknowledgments

This research was financially supported by National Natural Science Foundation of China (Nos: 41972088, 42002073 and 91962215), China Postdoctoral Science Foundation (2019M663138), and the Guangzhou Science and Technology Project (Grant No. 201707010422). We thank the staff of Geology Bureau for Nonferrous Metals of Guangdong Province for their help in the field. State Key Laboratory of Isotope Geochemistry, Guangzhou Institute of Geochemistry, Chinese Academy of Sciences (GIGCAS) is acknowledged for SIMS zircon U—Pb dating, major and trace element, In-situ Sr isotope analyses on plagioclase, and Sr–Nd–Pb analyses. The first author thanks the support of CSC Joint PhD Training Program for providing the living expenses in Canada. We would like to thank Xianhua Li for his editorial handling and Chuanlin Zhang and two anonymous reviewers for their cogent comments,which contributed the improvement of this paper.

Appendix A. Supplementary data

Supplementary data to this article can be found online at https://doi.org/10.1016/j.lithos.2021.106021.

References

Aldanmaz, E., Pearce, J.A., Thirlwall, M.F., Mitchell, J.G., 2000. Petrogenetic evolution of late Cenozoic, post-collision volcanism in western Anatolia, Turkey. J. Volcanol. Geotherm. Res. 102 (1–2), 67–95.
Anderson, D.L., 1994. The sublithospheric mantle as the source of continental flood basalts; the case against the continental lithosphere and plume head reservoirs. Earth Planet. Sci. Lett. 123, 269–280.
Chauvel, C., Hofmann, A.W., Vidal, P., 1992. HIMU-EM: the French Polynesian connection. Earth Planet. Sci. Lett. 110 (1–4), 99–119.
Chen, C.H., Lee, C.Y., Shinjo, R., 2008. Was there Jurassic paleo-pacific subduction in South China?: constraints from 40Ar/39Ar dating, elemental and Sr–Nd–Pb isotopic geochemistry of the Mesozoic basalts. Lithos 106, 83–92.
Chen, H., Xia, Q.K., Ingrin, J., Jia, Z.B., Feng, M., 2015. Changing recycled oceanic components in the mantle source of the Shuangliao Cenozoic basalts, NE China: new constraints from water content. Tectonophysics 650, 113–123.
Chen, H., Xia, Q.K., Ingrin, J., Deloule, E., Bi, Y., 2017. Heterogeneous source components of intraplate basalts from NE China induced by the ongoing Pacific slab subduction. Earth Planet. Sci. Lett. 459, 208–220.
DePAOLO, D.J., 1981. Trace element and isotopic effects of combined wallrock assimilation and fractional crystallization. Earth and planetary science letters 53 (2), 189–202.
De Paolo, D.J., Daley, E.E., 2000. Neodymium isotopes in basalts of the southwest basin and range and lithospheric thinning during continental extension. Chem. Geol. 169, 157–185.
Eby, G.N., 1992. Chemical subdivision of the A-type granitoids: petrogenetic and tectonic implications. Geology 20 (7), 641–644.
Elburg, M., Vroon, P., van der Wagt, B., et al., 2005. Sr and Pb isotopic composition of five USGS glasses (BHVO-2G, BIR-1G, BCR-2G, TB-1G, NKT-1G)[J]. Chem. Geol. 223 (4), 196–207.

Gan, C., Zhang, Y., Barry, T.L., He, J., Wang, Y., 2018. Jurassic metasomatised lithospheric mantle beneath South China and its implications: Geochemical and Sr-Nd isotope evidence from the Late Jurassic shoshonitic rocks. Lithos 320, 236–249.
Gao, S., Luo, T.C., Zhang, B.R., Zhang, H.F., Han, Y.W., Zhao, Z.D., Hu, Y.K., 1998. Chemical composition of the continental crust as revealed by studies in East China. Geochimica et Cosmochimica Acta 62 (11), 1959–1975.
Gilder, S.A., Keller, G.R., Luo, M., Goodell, P.C., 1991. Timing and spatial distribution of rifting in China. Tectonophysics 197, 225–243.
Guo, F., Fan, W.M., Li, C.W., Zhao, L., Li, H.X., Yang, J.H., 2012. Multi-stage crust–mantle interaction in SE China: Temporal, thermal and compositional constraints from the Mesozoic felsic volcanic rocks in eastern Guangdong–Fujian provinces. Lithos 150, 62–84.
Hofmann, A.W., White, W.M., 1982. Mantle plumes from ancient oceanic crust. Earth Planet Sci Lett 57, 421–436.
Hofmann, A.W., Jochum, K.P., Seufert, M., White, W.M., 1986. Nb and Pb in oceanic basalts: new constraints on mantle evolution. Earth and Planetary Science Letters 79, 33–45.
Huang, H.Q., Li, X.H., Li, Z.X., Li, W.X., 2013a. Intraplate crustal remelting as the genesis of Jurassic high-K granites in the coastal region of the Guangdong Province, SE China. J. Asian Earth Sci. 74 (280s), 74.
Huang, X.L., Niu, Y., Xu, Y.G., Ma, J.L., Qiu, H.N., Zhong, J.W., 2013b. Geochronology and geochemistry of Cenozoic basalts from eastern Guangdong, SE China: constraints on the lithosphere evolution beneath the northern margin of the South China Sea. Contributions to Mineralogy and Petrology 165 (3), 437–455.
Jahn, B.M., Zhou, X.H., Li, J.L., 1990. Formation and tectonic evolution of southeastern China and Taiwan: isotopic and geochemical constraints. Tectonophysics 183, 145–160.
Jiang, Y.H., Jiang, S.Y., Dai, B.Z., Liao, S.Y., Zhao, K.D., Ling, H.F., 2009. Middle to late Jurassic felsic and mafic magmatism in southern Hunan province, southeast China: implications for a continental arc to rifting. Lithos 107 (3–4), 185–204.
Jiang, Y.H., Zhao, P., Zhou, Q., Liao, S.Y., Jin, G.D., 2011. Petrogenesis and tectonic implications of Early Cretaceous S-and A-type granites in the northwest of the GanHang rift, SE China. Lithos 121 (1), 55–73.
Johnson, K.T.M., 1994. Experimental cpx/and garnet/melt partitioning of REE and other trace elements at high pressures: petrogenetic implications. Mineralogical Magazine A 58, 454–455.
Li, Z.X., Li, X.H., 2007. Formation of the 1300-km-wide intracontinental orogen and postorogenic magmatic province in Mesozoic South China: a flat-slab subduction model. Geology 35, 179–182.
Li, X.H., Li, Z.X., Zhou, H.W., Liu, Y., Kinny, P.D., 2002. U–Pb zircon geochronology, geochemistry and Nd isotopic study of Neoproterozoic bimodal volcanic rocks in the Kangdian Rift of South China: implications for the initial rifting of Rodinia. Precambrian Res. 113, 135–154.
Li, X.H., Chung, S.L., Zhou, H., Lo, C.H., Liu, Y., Chen, C.H., 2004. Jurassic intraplate magmatism in southern Hunan-eastern Guangxi: 40Ar/39Ar dating, geochemistry, Sr-Nd isotopes and implications for the tectonic evolution of SE China. Geol. Soc. Lond. Spec. Publ. 226 (1), 193–215.
Li, X.H., Liu, Y., Li, Q.L., Guo, C.H., Chamberlain, K.R., 2009. Precise determination of Phanerozoic zircon Pb/Pb age by multicollector SIMS without external standardization. Geochem. Geophys. Geosyst. 10.
Li, X.H., McCulloch, M.T., 1998. Geochemical characteristics of Cretaceous mafic dikes from northern Guangdong, SE China: Age, origin and tectonic significance. Mantle dynamics and plate interactions in East Asia 27, 405–419.
Li, X., Tang, G., Gong, B., Yang, Y., Hou, K., Hu, Z., Li, Q., Liu, Y., Li, W., 2013. Qinghu zircon: a working reference for microbeam analysis of U-Pb age and Hf and O isotopes. Chin. Sci. Bull. 58, 4647–4654.
Li, Z., Qiu, J.S., Yang, X.M., 2014. A review of the geochronology and geochemistry of Late Yanshanian (Cretaceous) plutons along the Fujian coastal area of southeastern China: implications for magma evolution related to slab break-off and rollback in the Cretaceous. Earth Sci. Rev. 128, 232–248.
Li, Q., Zhao, K.D., Lai, P.C., Jiang, S.Y., Chen, W., 2018. Petrogenesis of Cretaceous volcanic-intrusive complex from the giant Yanbei tin deposit, South China: implication for multiple magma sources, tin mineralization, and geodynamic setting. Lithos 296, 163–180.
Liang, X.R., Wei, G.J., Li, X.H., Liu, Y., 2003. Precise measurement of 143Nd/144Nd and Sm/Nd ratios using multiple-collectors inductively coupled plasma-mass spectrometer (MCICPMS). Geochimica 32, 91–96.
Liu, X., Fan, H.R., Santosh, M., Hu, F.F., Yang, K.F., Li, Q.L., Yang, Y.H., Liu, Y.S., 2012. Remelting of Neoproterozoic relict volcanic arcs in the Middle Jurassic: implication for the formation of the Dexing porphyry copper deposit, Southeastern China. Lithos 150, 85–100.
Liu, L., Xu, X., Xia, Y., 2014. Cretaceous Pacific plate movement beneath SE China: Evidence from episodic volcanism and related intrusions. Tectonophysics 614, 170–184.
Liu, L., Xu, X., Xia, Y., 2015a. Asynchronizing paleo-Pacific slab rollback beneath SE China: insights from the episodic Late Mesozoic volcanism. Gondwana Res. https://doi.org/10.1016/j.gr.2015.09.009.
Liu, J., Xia, Q.K., Deloule, E., Ingrin, J., Chen, H., Feng, M., 2015b. Water content and oxygen isotopic composition of alkali basalts from the Taihang Mountains, China: recycled oceanic components in the mantle source. Journal of Petrology 56 (4), 681–702.
Liu, P., Cheng, Y.B., Mao, J.W., Wang, X.Y., Yao, W., Cheng, X.T., Zeng, X.J., 2015. Zircon U-Pb age and Hf isotopic characteristics of granite from the Tiandong tungsten-Sn polymetallic deposit in eastern Guangdong Province and its signifcance: Acta Geological Sinica. 89, pp. 1244–1257 (inChinese with English abstract).
Liu Cheng, P., 2016c. Zircon U-Pb age and Hf isotopic characteristics of granite fromthe Tiandong tungsten-Sn polymetallic deposit in eastern Guangdong Province and its signifcance: Acta Geological Sinica. 80, pp. 1244–1257 (inChinese with English abstract).
Ludwig, K.R., 2003. User's Manual for Isoplot/Ex Version 3.00—A Geochronology Toolkit for Microsoft Excel. Berkeley Geochronology Center Special Publication 4, 1–70.
Ma, L., Wang, Q., Kerr, A.C., Yang, J.H., Xia, X.P., Ou, Q., Sun, P., 2017. Paleocene (c. 62 Ma) leucogranites in southern Lhasa, Tibet: products of syn-collisional crustal anatexis during slab roll-back? Journal of Petrology 58 (11), 2089–2114.
Mathieu, L., De Vries, B.V.W., Holohan, E.P., Troll, V.R., 2008. Dykes, cups, saucers and sills: Analogue experiments on magma intrusion into brittle rocks. Earth and Planetary Science Letters 271 (1-4), 1–13.
Mao, J.W., Cheng, Y.B., Chen, M.H., Pirajno, F., 2013. Major types and time–space distribution of Mesozoic ore deposits in South China and their geodynamic settings. Mineral. Deposita 48, 267–294.
Meng, L., Li, Z.X., Chen, H., Li, X.H., Wang, X.C., 2012. Geochronological and geochemical results from Mesozoic basalts in southern South China Block support the flat-slab subduction model. Lithos 132, 127–140.
McKenzie, D.P., 1989. Some remarks on the movement of small volume melt fractions in the mantle. Earth and Planetary Science Letters 95, 53–72.
Niu, Y.L., O'Hara, M.J., 2003. Origin of ocean island basalts: A new perspective from petrology, geochemistry, and mineral physics considerations. Journal of Geophysical Research: Solid Earth 108 (B4).
Niu, Y.L., 2008. The origin of alkaline lavas. SCIENCE-NEW YORK THEN WASHINGTON 320 (5878), 883.
McKenzie, D., O'Nions, R.K., 1991. Partial melt distributions from inversion of rare earth element concentrations. Journal of Petrology 32, 1021–1091.
Orejana, D., Villaseca, C., Billström, K., Paterson, B.A., 2008. Petrogenesis of Permian alkaline lamprophyres and diabases from the Spanish central system and their geodynamic context within western Europe. Contrib. Mineral. Petrol. 156 (4), 477–500.
Pang, K.N., Chung, S.L., Zarrinkoub, M.H., Mohammadi, S.S., Yang, H.M., Chu, C.H., Lo, C.H., 2012. Age, geochemical characteristics and petrogenesis of Late Cenozoic intraplate alkali basalts in the Lut–Sistan region, eastern Iran. Chemical Geology 306, 40–53.
Peacock, S.M., Wang, K., 1999. Seismic consequences of warm versus cool subduction metamorphism: examples from southwest and northeast Japan. Science 286 (5441), 937–939.
Plank, T., Langmuir, C.H., 1998. The chemical composition of subducting sediment and its consequences for the crust and mantle. Chemical geology 145 (3-4), 325–394.
Polat, A., Hofmann, A.W., Rosing, M.T., 2002. Boninite-like volcanic rocks in the 3.7–3.8 Ga Isua greenstone belt, West Greenland: geochemical evidence for intra-oceanic subduction zone processes in the early Earth. Chem. Geol. 184, 231–254.
Qiu, Z., Li, S., Yan, Q., Wang, H., Wei, X., Li, P., Wang, L.M., Bu, A., 2017. Late Jurassic Sn metallogeny in eastern Guangdong, SE China coast: evidence from geochronology, geochemistry and Sr–Nd–Hf–S isotopes of the Dadaoshan Sn deposit. Ore Geol. Rev. 83, 63–83.
Rudnick, R.L., Gao, S., 2003. Composition of the continental crust. Treatise Geochem. 3, 1–64.
Shu, L.S., Zhou, X.M., Deng, P., Wang, B., Jiang, S.Y., Yu, J.H., Zhao, X.X., 2009. Mesozoic tectonic evolution of the Southeast China Block: new insights from basin analysis. J. Asian Earth Sci. 34 (3), 376–391.
Sun, S.S., McDonough, W.E., 1989. Chemical and isotopic systematics of oceanic basalts: Implications for mantle composition and processes. In: Saunders, A.D., Norry, M.J. (Eds.), Magmatism in the Ocean Basins. Geological Society of London. Special Publication. 42, pp. 313–345.
Veevers, J.J., 2004. Gondwanaland from 650–500 Ma assembly through 320 Ma merge in Pangea to 185–100 Ma breakup: supercontinental tectonics via stratigraphy and radiometric dating. Earth Science Reviews 68, 1–132.
Wei, G.J., Liang, X.R., Li, X.H., Liu, Y., 2002. Precise measurement of Sr isotopic composition of liquid and solid base using (LP)MC-ICPMS. Geochimica 31, 295–299.
Winchester, J.A., Floyd, P.A., 1977. Geochemical discrimination of different magma series and their differentiation products using immobile elements. Chemical geology 20, 325–343.
Wong, J., Sun, M., Xing, G.F., Li, X.-H., Zhao, G.C., Wong, K., Yuan, C., Xia, X.P., Li, L.M., Wu, F.Y., 2009. Geochemical and zircon U–Pb and Hf isotopic study of the Baijuhuajian metaluminous A-type granite: extension at 125–100 Ma and its tectonic significance for South China. Lithos 112, 289–305.
Workman, R.K., Hart, S.R., 2005. Major and trace element composition of the depleted MORB mantle (DMM). Earth Planet. Sci. Lett. 231 (1–2), 53–72.
Xia, Q.K., Liu, J., Liu, S.C., Kovacs, I., Feng, M., Dang, L., 2013. High water content in Mesozoic primitive basalts of the North China Craton and implications on the destruction of cratonic mantle lithosphere. Earth and Planetary Science Letters 361, 85–97.
Xie, X., Xu, X., Zou, H., Xing, G., 2001. Trace element and Nd-Sr-Pb isotope studies of Mesozoic and Cenozoic basalts in coastal area of se china. Acta Petrologica Sinica 17 (4), 617–628.
Xu, X.C., Yue, S.C., 1999. Source material and metallization of tin (tungsten, copper) polymetallic deposits in eastern Guangdong Province. J. Hefei Univ. Technol. 34 (1), 81–92 (in Chinese with English abstract).
Yan, Q.H., Li, S.S., Qiu, Z.W., Wang, H., Wei, X.P., Dong, R., Zhang, X.Y., 2017. Geochronology, geochemistry and Sr–Nd–Hf–S–Pb isotopes of the early cretaceous Taoxihu Sn deposit and related granitoids, SE China. Ore Geol. Rev. 89, 350–368.
Yan, Q.H., Wang, H., Qiu, Z.W., Wei, X.P., Li, P., Dong, R., Zhou, K.L., 2018. Origin of Early Cretaceous A-type granite and related Sn mineralization in the Sanjiaowo deposit, eastern Guangdong, SE China and its tectonic implication. Ore Geol. Rev. 93, 60–80.
Yan, Q.H., Wang, H., Chi, G., 2020. Pulsed magmatic fluid releasing in the formation of the Taoxihu Sn polymetallic deposit, eastern Guangdong, SE China: evidence from fluid inclusions, cassiterite U–Pb geochronology, and stable isotopes. Ore Geol. Rev. 126, 103724.

Yang, S.Y., Jiang, S.Y., Zhao, K.D., Jiang, Y.H., Ling, H.F., Luo, L., 2012. Geochronology, geochemistry and tectonic significance of two Early Cretaceous A-type granites in the Gan-Hang Belt, Southeast China. Lithos 150, 155–170.

Zhang, Hu, 2020. Estimation of isotopic reference values for pure materials and geological reference materials. At. Spectrosc. 41, 93–102.

Zhang, L., Ren, Z.Y., Wu, Y.D., et al., 2018. Sr isotope measurement of basaltic glasses by LA-MC-ICP-MS based on a linear relationship between analytical bias and Rb/Sr ratios[J]. Rapid Commun. Mass Spectrom. 8011 doi:10.1002/rcm.

Zhou, X.M., Li, W.X., 2000. Origin of late Mesozoic igneous rocks in southeastern China: implications for lithosphere subduction and underplating of mafic magmas. Tectonophysics 326, 269–287.

Zhou, X.M., Sun, T., Shen, W.Z., 2006. Petrogenesis of Mesozoic Granitoids and Volcanic Rocks in South China: A Response to Tectonic Evolution. Episodes 29 (1), 26–33.

Zhao, J.H., Zhou, M.F., 2007. Geochemistry of Neoproterozoic mafic intrusions in the Panzhihua district (Sichuan Province, SW China): Implications for subduction-related metasomatism in the upper mantle. Precambrian Research 152 (1-2), 27–47.

Zhou, Z.M., Ma, C.Q., Xie, C.F., Wang, L.X., Liu, Y.Y., Liu, W., 2016. Genesis of highly fractionated I-type granites from Fengshun complex: implications to tectonic evolutions of South China. J. Earth Sci. 27, 444–460.

Zou, H., Zindler, A., 1996. Constraints on the degree of dynamic partial melting and source composition using concentration ratios in magmas. Geochimica et Cosmochimica Acta 60, 711–717.